Proceedings of ASME Turbo Expo 2011
GT2011
June 6-10, 2011, Vancouver, British Columbia, Canada

GT2011-45627

INTEGRATED OGV DESIGN FOR AN AGGRESSIVE S-SHAPED COMPRESSOR TRANSITION DUCT

A D Walker, A G Barker and J F Carrotte
Dept. of Aero. and Auto. Engineering,
Loughborough University, UK
Email: a.d.walker@lboro.ac.uk

J J Bolger and M J Green
Rolls-Royce plc, Derby, UK

ABSTRACT

Within gas turbines the ability to design shorter aggressive S-shaped ducts is advantageous from a performance and weight saving perspective. However, current design philosophies tend to treat the S-shaped duct as an isolated component, neglecting the potential advantages of integrating the design with the upstream or downstream components. In this paper such a design concept is numerically developed in which the upstream compressor outlet guide vanes are incorporated into the first bend of the S-shaped duct. Positioning the vane row within the first bend imparts a strong radial gradient to the pressure field within the vane passage. Tangential lean and axial sweep are employed such that the vane geometry is modified to exactly match the resulting inclined static pressure field. The integrated design is experimentally assessed and compared to a conventional non-integrated design on a fully annular low speed test facility incorporating a single stage axial compressor. Several traverse planes are used to gather five-hole probe data which allow the flow structure to be examined through the rotor, outlet guide vane and within the transition ducts. The two designs employ almost identical duct geometry, but integration of the vane row reduces the system length by 21%. Due to successful matching of the static pressure field, the upstream influence of the integrated vane row is minimal and the rotor performance is unchanged. Similarly the flow development within both S-shaped ducts is similar such that the circumferentially averaged profiles at duct exit are almost identical, and the operation of a downstream component would be unaffected. Overall system loss remains nominally unchanged despite the inclusion of lean and sweep and a reduction in system length. Finally, the numerical design predictions show good agreement with the experimental data thereby successfully validating the design process.

NOMENCLATURE

A	-	Area
Cp	-	Static pressure rise coefficient
h	-	Passage height
IGV	-	Inlet Guide Vane
IOGV	-	Integrated Outlet Guide Vane
L	-	Duct length
N	-	Rotor speed
OGV	-	Outlet Guide Vane
P	-	Total pressure
p	-	Static pressure
r, R	-	Radius
r_m	-	Mean radius
r_i	-	Inner wall (hub) radius
r_o	-	Outer wall (casing) radius
U, V ,W	-	Axial, radial and tangential velocity components in cylindrical-polar coordinates
U_L, V_L	-	Velocity components relative to local traverse plane
x	-	Axial coordinate
y+	-	Dimensionless wall distance
α	-	Kinetic energy flux coefficient
ρ	-	Density
ϕ	-	Flow coefficient (V_{axial}/U_{blade})
ψ	-	Work coefficient ($\Delta H/U_{blade}^2$)
θ	-	Traverse plane angle relative to axial direction
λ	-	Total pressure loss coefficient

Superscripts

-	-	Area weighted spatial average
~	-	Mass weighted spatial average

Subscripts

A–H, J	-	Measurement planes
L	-	Local plane

INTRODUCTION

To optimize the performance of multi-spool gas turbine compressor systems the diameter of each spool must reduce as the air density increases. In order to accomplish this, the annular transition duct connecting the low and high pressure compressor spools generally takes the form of an S-shape. In modern, high pressure ratio aircraft engines this radius change is increasing and must be accomplished in the shortest possible length to minimize engine length/weight. Consequently there is a need to design progressively more aggressive S-shaped ducts. However, within such ducts flow separation must be avoided if, in line with overall cycle performance, the stagnation pressure loss is to be minimized and the downstream compressor performance not adversely affected. Furthermore, what appears to be a relatively simple geometric shape actually poses some significant aerodynamic challenges because of the complex nature of the flow field which develops under the combined influence of pressure gradient and streamline curvature effects.

As the flow follows a curved path through the duct a modification to the static pressure field occurs (Figure 1). Across the first bend a radial pressure gradient is required to turn the flow inwards such that the pressure close to the outer casing is higher than that adjacent to the inner. Within the second bend the flow is returned to the axial direction and so the radial pressure gradient is reversed. As a consequence, streamwise pressure gradients are generated that influence the flow field development in various regions of the duct, including the boundary layers that develop along the duct walls. In particular, for a compressor transition duct, the flow is subject to an adverse pressure gradient along most of the inner wall increasing the likelihood of separation. Additionally, the turbulent flow field is directly influenced by the streamline curvature that is undertaken by the flow. As described by Bradshaw[1] the imbalance that exists between the centripetal acceleration of a turbulent fluid element and the surrounding pressure field gives rise, over a convex surface, to reduced turbulence levels so that turbulent mixing is inhibited and turbulent stresses reduced. Alternatively, over a concave surface turbulent mixing and the associated stresses are increased. In the case of a boundary layer, for example, the gradient of shear stress in the near wall region enables the near wall fluid to advance against the increasing pressure. Hence modification to the turbulent flow field due to streamline curvature effects can be significant, particularly in regions where the flow is close to separation.

Several parameters can be used to quantify, geometrically, the aggressiveness of an S-shape duct. For example, with reference to Figure 1, the non-dimensional radius change ($\Delta R/L$) reflects the severity of the curvature induced pressure gradients. The duct area ratio (A_2/A_1) reflects the bulk deceleration (or acceleration) of the fluid and, in a similar way to a conventional diffuser, the non-dimensional length (L/h_1) over which this is undertaken will dictate the axial pressure gradient. These combine to set the magnitude of the adverse pressure gradient along the inner wall of the second bend where separation is most likely. Aerodynamically other factors should also be considered such as the duct inlet (turbulence structure, boundary layer thickness etc.) and exit conditions. The presence of an upstream compressor, and in particular the presence of outlet guide vane (OGV) wakes, can have a notable effect on performance. Bailey et al.[2] and Karakasis et al.[3] both measured a notable increase in duct loss due to the presence of compressor generated inlet conditions. Karakasis et al.[3] reported that the OGV wakes pool on the hub wall, forming contra-rotating streamwise vortex pairs. These cause the hub boundary layer fluid to be pumped into the higher velocity free stream, thus raising the mixing loss. However, the increased turbulent mixing can also be beneficial as it promotes the transfer of higher momentum core flow into the boundary layers. This phenomenon has been utilized for many years to enable the design of more aggressive combustor pre-diffusers (see for example Carrotte et al.[4]). Indeed, Walker et al.[5] used an integrated OGV/pre-diffuser design to enhance this effect to enable a diffuser to remain attached at a level of loading (area ratio) which would normally result in flow separation. In S-shaped ducts the increased turbulent mixing has also been observed to reduce the likelihood of separation [2, 6] but the phenomenon is modified and enhanced by the radial pressure gradient present in the first bend. For example, Britchford[6] commented that the radial pressure gradient affects the low momentum wake fluid to a greater extent than the core flow thereby driving it towards the inner casing. Although a deficit in total pressure exists between the wake flow and the core flow the wake flow still has a higher total pressure than the boundary layer and thus acts to re-energize the latter.

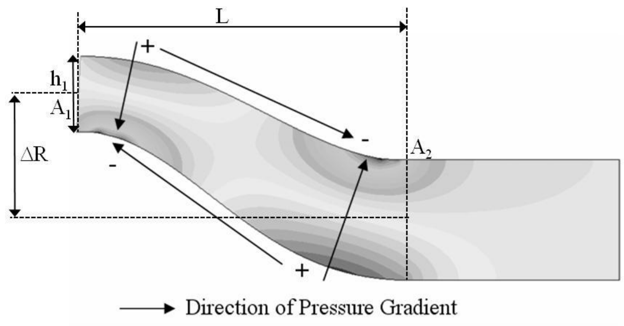

Figure 1: Static Pressure in an S-shaped Duct

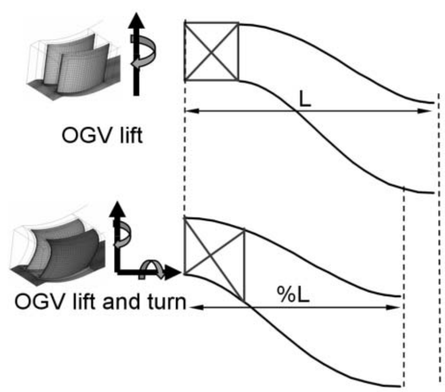

Figure 2: Integrated OGV Concept

In the current investigation the upstream compressor OGV row was integrated into the first bend of an aggressive S-duct, as illustrated in Figure 2, giving rise to a significant length saving without increasing the likelihood of flow separation. To do this the OGV must incorporate an amount of tangential lean in order to impart a radial force component and match the required static pressure field within the first bend. Lean (sometimes termed dihedral) is essentially movement of the aerofoil section normal to the chord line. With the ability to use 3D CFD to design complex 3D blading it is not unusual for modern engines to incorporate blade lean or sweep to impart some radial deflection on the flow. Sweep is defined as movement of the aerofoil section parallel to the chord. For example, Smith[7] and Wadia et al.[8] discuss the use of lean and sweep to reduce OGV hub Mach numbers, deflect the flow in a radial direction and reduce the loading in the downstream duct. In both cases the OGV were not integral with the duct. However, Britchford et al.[9] studied an annular S-shaped duct positioned immediately downstream of a low-pressure fan OGV (Figure 3). They examined the use of OGV lean and sweep to impart a radial component and help turn a portion of the flow into the core.

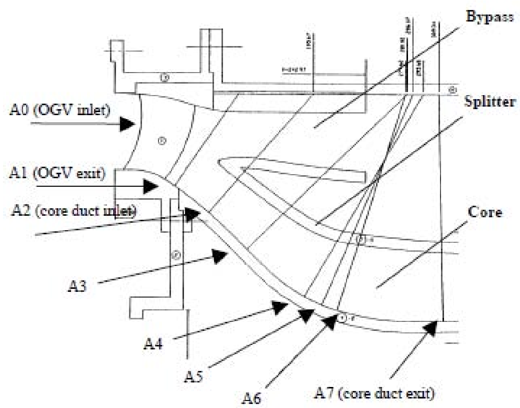

Figure 3: Integrated OGV Design[9]

The current paper describes a similar approach to integrate the OGV into the first bend of an aggressive S-duct designed to transfer the flow from a low to high pressure compressor. The design was numerically developed and evaluated before being assessed on a low-speed test facility where its performance was compared to a datum S-shaped duct in which the OGV row was positioned upstream of the duct (Figure 4). The objectives of the work can be summarized as:

- Integrate the OGV into the first bend of the duct thereby saving at least 20% of the system length,
- Maintain the rotor exit pressure field such that the rotor performance is unaffected, and
- Retain the downstream (conventional) duct geometry and level of radial turning such that the exit flow is unchanged and the performance of a downstream compressor unaffected.

DESIGN METHODOLOGY

Many authors such as Denton and Xu[10] have discussed the exploitation of 3D flow effects in turbomachinery design, including the use of lean and sweep to reduce blade loading in the hub or tip regions. Indeed Gallimore et al.[11] employed the use of sweep and dihedral (lean) in the blading design of a multistage axial flow compressor. However, the aim in the current work was to lean the OGV in order to match the static pressure field in the first bend of an S-shaped duct, thereby enabling the OGV to be positioned within the bend and have minimal impact on the system aerodynamics. At high Reynolds numbers the flow curvature is mainly balanced by gradients in pressure. For example, a radial pressure gradient ($\frac{1}{\rho}\frac{\partial p}{\partial r}$) balances any acceleration associated with the curvature about the engine axis (W^2/r). In the case of a stator vane curvature within the blade to blade plane gives rise to an acceleration (V_{rel}^2/R_{blade}) which is balanced by lines of constant static pressure that are radial (Figure 5a). Similarly, curvature in the streamwise plane gives rise to an acceleration (U^2/R_{duct}) which is balanced by circumferential lines of constant static pressure (Figure 5b). Generally, in a parallel passage such as in a conventional compressor the blade to blade curvature is dominant such that, to ensure constant spanwise loading, the blades are located radially. However, in the first bend of an S-duct the streamwise curvature has a significant affect and, in the current S-duct design, was of a similar magnitude to the blade to blade curvature. Hence the OGV needed to be leaned (Figure 5c) in order to impart a radial force component and match the required static pressure field within the bend. A lean of approximately 45° was required, although the exact angle changes as the streamwise curvature changes with distance from the hub. Nevertheless this highlights the basic method used to integrate the OGV into the first bend of the S-duct.

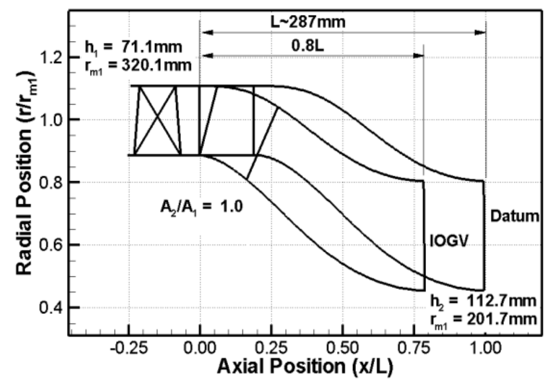

Figure 4: Datum and Integrated OGV Geometry

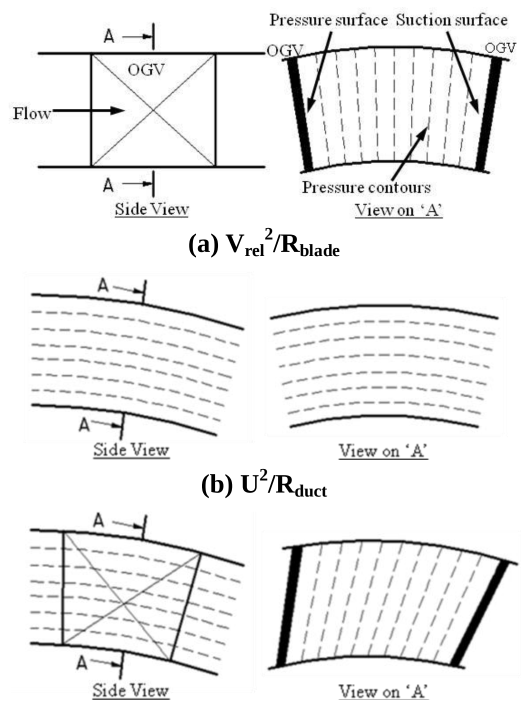

(a) V_{rel}^2/R_{blade}

(b) U^2/R_{duct}

(a)+(b) → blade lean

Figure 5: Static Pressure Contours of Curved Flows

OGV AND DUCT DESIGN

Datum – In the datum design the duct begins at the OGV exit with both components being coupled in the design process via an inviscid streamline curvature code. However, no attempt was made to integrate their design. Nevertheless, the datum S-shaped design intent was to be at the limit of aerodynamic loading – i.e. close to, but not actually, separated. The design parameters for both ducts are given in Table 1 and specification of the mean radius was achieved via the trigonometric function:

$$r_m = a_1 + a_2 \cos\left(\pi \frac{x}{L}\right) - a_3 \sin^2\left(\pi \frac{x}{L}\right) \tag{1}$$

The aerodynamic duty of the upstream compressor was chosen to be typical of the rear stages of a low-pressure compressor such that representative wakes and secondary flows would be generated as inlet conditions to the OGV. The OGV itself was designed using proprietary geometry generation tools and the 2D blade-to-blade solver MISES[12] to generate aerofoil profiles at various heights up the blade span. 3D design computations were performed using the Rolls-Royce Hydra CFD code[13], a hybrid unstructured mesh solver. The code was fully parallel and used a pre-conditioned five-step Runge-Kutta time marching scheme with four levels of multi-grid to speed convergence. Hybrid COH meshes were used for the blading with simulated fillet radii and fully-gridded rotor tip clearances. The Spalart-Allmaras turbulence model was used, and rotating and stationary blade rows were joined using a non-reflective mixing plane. However, this meant that the unsteadiness associated with the upstream rotor did not pass into the OGV row and duct. The grid size corresponded to approximately 500k cells per blade row, with the y+ on all surfaces being in the region of 1 - 2. Grid resolution within the duct was typically 70 cells in the pitchwise and radial directions and 300 cells in the axial direction.

	L_{system}/h_1	L_{duct}/h_1	$\Delta R/L_{duct}$	A_2/A_1
Datum	4.0	3.2	0.5	1.0
IOGV	3.2	3.2	0.5	1.0

Table 1: S-Shaped Duct Design Parameters

IOGV – As shown in Figure 4 the integrated design reduced the system length by approximately 21% (whilst maintaining the same radius change). Although a stated aim was to maintain the shape of the duct the profile through the integrated OGV passage was altered slightly to maintain the area ratio across the OGV (and hence the same diffusion levels and loss). However, downstream of this the duct profile remained identical to the datum. The IOGV generic blade section design was retained from the datum design with only minor changes being made to blade inlet and exit angles and chord. Positioning the OGV within the first bend means that the strong radial component to the pressure field must be accommodated. The OGV was therefore leaned to match the resulting inclined contours of static pressure. Both tangential lean and axial sweep were applied and 3D stacking of the OGV was investigated in a parametric CFD study. This included variations of sweep, lean, profile re-camber (adjustment of the leading/trailing edge to more closely match the local flow direction) and the blend of 3D endwall stacking into the mid-span regions. As an example, Figure 6 shows the predicted static pressure contours on a plane normal to the flow mid-way through the OGV passage.

The design predictions suggested an improvement in compressor stage efficiency of 0.8% over the datum which implies less loss in the OGV as the rotor is identical. However, the use of a mixing plane between the rotor and OGV removes differences in the spatial structure of the rotor back pressure which has the potential to alter the rotor performance. Nevertheless, a flow range greater than -10% (in the flow coefficient) was demonstrated by the CFD before the onset of numerical instabilities and it is expected that the compressor could be pushed to lower exit flows if required. Although not shown the stage characteristics (speed curve) over this range were identical for the two designs. Additionally, in line with the design intent, the predictions also revealed the rotor exit flow for the datum and IOGV designs to be virtually identical.

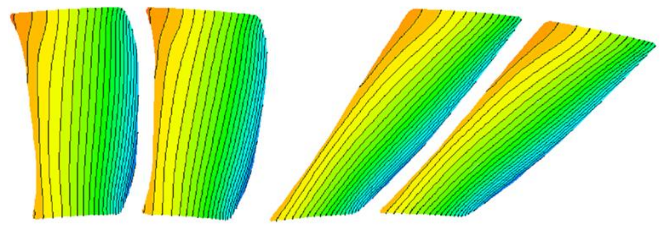

(a) Datum (b) IOGV

Figure 6: Static Pressure Contours in OGV Row

S-SHAPED DUCT PRE-TEST CFD ASSESSMENT

The numerical design of the OGV/duct was accomplished using a tried and tested methodology which employs the one equation Spalart-Allmaras turbulence model and fully resolves the boundary layers as they develop on the OGV. Including the S-shaped duct in this model was important to provide the OGV with a representative downstream pressure field. However, it is believed that the fidelity of the turbulence model was insufficient to accurately assess the development of the flow within the S-shaped duct. This is important as the design philosophy was such that S-shaped ducts should be aggressive to the point that the flow is close to, but not actually, separated. Consequently, before committing to an experimental test program there was a need to confirm this numerically with a high level of confidence. The various factors which influence the flow field development within an S-shaped duct provide a notable challenge for numerical methods. The studies of Ortiz-Dueanas et al.[14] and Karakasis et al.[3] reported that a Spalart-Allmaras and a k-ω SST turbulence model both gave solutions which differed to experimental data in the near wall regions. This is not surprising. Eddy-viscosity models use the Boussinesq hypothesis to compute the Reynolds stresses. This assumes isotropic turbulent viscosity which is certainly not the case in the presence of strong streamline curvature. To capture the impact of streamline curvature on the turbulence field, Britchford et al.[6] showed that a Reynolds stress transport model is more accurate although still shows some minor differences to experimental data. Furthermore, with compressor generated inlet conditions, wake mixing through the transition duct must also be correctly captured in order to obtain the correct wake characteristics and therefore any migration of wake fluid towards the critical inner wall. Eddy-viscosity models have been observed to be less accurate in unconfined flows such as far wakes and mixing layers as the rate of production of turbulent kinetic energy can be much less than the rate of dissipation. Thus the duct flow was also predicted using the commercial CFD code Fluent (v6.3), a Reynolds stress turbulence closure and a standard wall function. Directly resolving the boundary layer was considered but was deemed both computationally too expensive and limiting in the choice of turbulence model. A true low Reynolds number wall modeling approach was unavailable with the Reynolds stress turbulence model in the version of Fluent used. Additionally Bradshaw[1] argues that curvature will affect the outer region more than the near wall region of the boundary layer. Computing this region with a Reynolds stress model was deemed more important than fully resolving the inner region. Hence a standard wall function was deemed acceptable.

To further reduce computational expense the OGV were not included in the prediction and the domain was reduced to a single OGV (7.5°) sector with periodic end walls. After grid refinement the final mesh had dimensions 180x80x45 in the axial, radial, circumferential directions. For the standard wall function to be valid care was taken to ensure grid density near the walls resulted in y+ value greater than 30-60 with a maximum value around 100. Velocity inlet conditions were taken directly from the OGV design predictions (Figure 7). Turbulence data were computed from typical turbulence intensities for the wake (12%), bulk (2.5%) and boundary layer (8%) regions with a length scale based on the width of the wake (~5mm). It must be noted that, as in the compressor/OGV design predictions, this methodology omits the unsteadiness generated by the rotor wakes. However, it is likely that the effect of this would be most notable in the OGV row rather than the downstream duct. In the post-test predictions (see later) the inlet conditions were taken from the measured OGV exit data and any modification of the mean flow field should therefore be included; at least sufficiently for a time-averaged prediction.

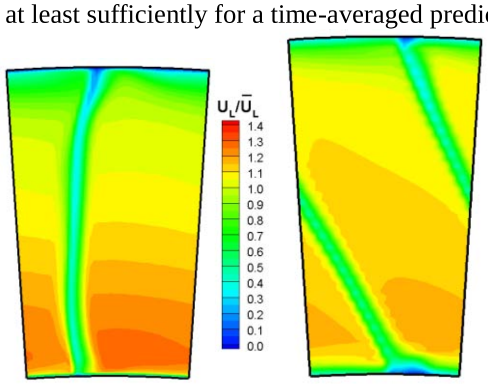

(a) Datum **(b) IOGV**

Figure 7: Normal Velocity at OGV Exit – Design CFD

The conventional datum design had been previously assessed experimentally and was known to be fully attached. Therefore the main aim of the pre-test CFD was to ensure the IOGV design had a similar level of aerodynamic loading and operated in a fully attached condition. This was confirmed by examination of the shear stress on the critical inner wall. Figure 8 illustrates an un-rolled projection of the inner wall showing that, in the critical second bend, the shear stress for the IOGV design does not fall below that of the datum. Hence it can be concluded that the IOGV design is no closer to separation. Furthermore, examination of the velocity contours at plane E (x/L~0.62) and duct exit (Figures 9 and 10) highlight the similarity of the predicted flow field development within both ducts. (Refer to Figure 11 for location of plane E).

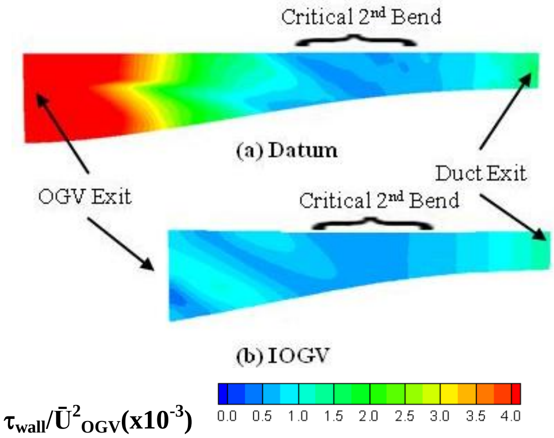

Figure 8: Predicted Wall Shear Stress on Inner Wall

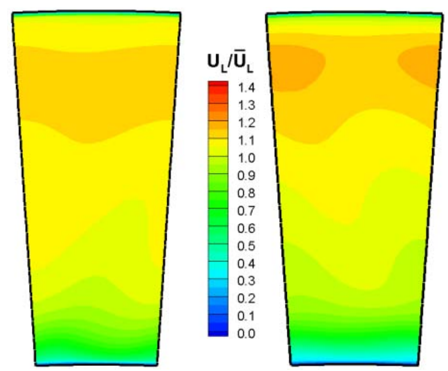

(a) Datum **(b) IOGV**

Figure 9: Predicted Velocity Contours at Plane E

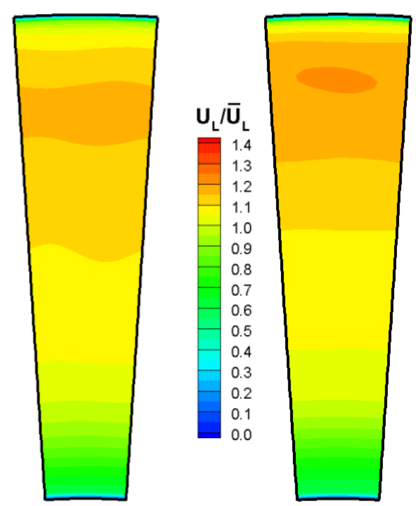

(a) Datum **(b) IOGV**

Figure 10: Predicted Velocity Contours at Duct Exit

EXPERIMENTAL FACILITY

All experimental data were obtained on a low speed test facility operating at nominally atmospheric conditions (Figures 11-12). Air was drawn into a large inlet plenum above the vertically mounted facility, before passing through an inlet flare and honeycomb flow straightener. The air was then accelerated over a bell-mouth intake section prior to passing into the test section which comprised a single stage axial compressor (with inlet guide vanes, a rotor and OGV) along with the S-shaped duct. The mean radius of the IGV and rotor was 320.1mm with a passage height of 71.1mm (h_1). The IGV row provided 10° of swirl onto the rotor which operated at a fixed non-dimensional mass flow condition ($m\sqrt{(RT)}/AP$) and speed ($(N\pi D/\sqrt{(\gamma RT)})$ corresponding to a flow coefficient of $\phi = 0.55$ and a work coefficient of $\psi = 0.4$. This resulted in a mass flow of approximately $6.3kgs^{-1}$ and an axial velocity through the blade rows of approximately $33ms^{-1}$ (Mach No. 0.1). Cumpsty[15] reports that for OGV Reynolds numbers below $1.5x10^5$ an undesirable separation bubble may develop on the suction surface of the OGV. In the present experiment the OGV Reynolds number was in excess of $2.0x10^5$ and therefore sufficiently high to avoid this. Further, the Reynolds number sensitivity of the OGV row was also suppressed by the presence of the relatively high levels of turbulence (>3%) generated by the rotor. Consequently, the wake mixing within the downstream S-shaped duct was well represented.

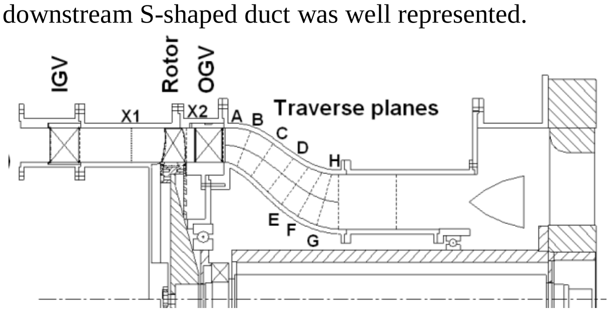

(a) Datum

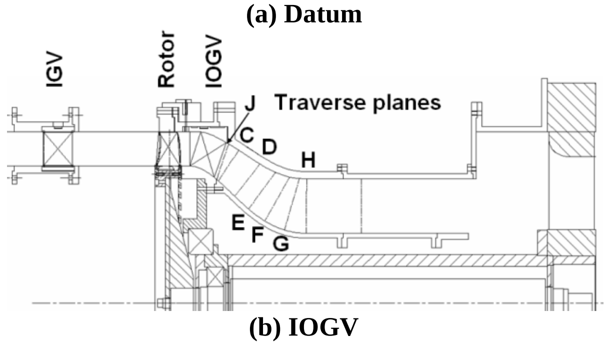

(b) IOGV

	A	B	J	C	D	E	F	G	H
x/L	0.0	0.17	0.28	0.33	0.49	0.62	0.75	0.88	1.0

Figure 11: S-Duct Test Section and Traverse Planes

In an aero engine a second compressor is typically located downstream of the S-shaped duct. This level of complexity was beyond the scope of the current work but it was noted that the downstream geometry has the potential to modify the duct flow. Therefore a settling length equal to 3.5 duct exit heights was used for both duct designs. This was sufficient to ensure the static pressure profile emanating from the ducts became radially uniform prior to the flow interacting with the rig exit throttle. Downstream of this the flow passed into a sub floor plenum and through a centrifugal fan before exhausting to atmosphere. The combination of the throttle and the fan were used to ensure that the compressor was maintained on the desired operating condition.

(a) Rig Assembly

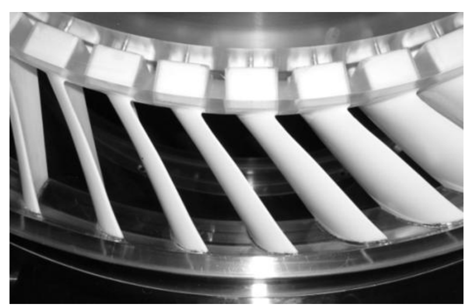

(b) IOGV

Figure 12: Test Rig Photographs

Information on the mean flow field was obtained using miniature five-hole pressure probes, of approximately 1.75mm diameter, suitably calibrated and employed in a non-nulled mode as outlined by Wray and Carrotte[16]. Measurements were performed on up to 11 traverse planes within the inlet section, S-shaped duct and settling length (Figure 11). The axial location of the planes are given with respect to the duct inlet (i.e. OGV exit for the datum and OGV inlet for the IOGV design). Thus, for the two designs, stations with the same letter are in identical locations with respect to the duct curvature. Each plane was aligned normal to the duct centre line and movement of the probe, across the annular passage, was obtained using a linear stepper motor. Circumferential movement was obtained by mounting the IGV and OGV rows within carrier rings such that the blade rows could be indexed circumferentially. This enabled area traverses of the flow field to be constructed. Measurements at the traverse planes were also complemented by 40 static pressure tappings located along the hub and casing walls.

DATA REDUCTION, ANALYSIS AND ERRORS

All the measurements were corrected to standard day conditions (P_{amb} = 101325 Nm^{-2}, T_{amb} = 288.15 K) and in all cases the velocities were measured in a local co-ordinate system (Figure 13). This consisted of vectors normal to the traverse plane (U_L), in the line of the measurement plane (V_L) and circumferentially around the duct (W_L). Typically, data is presented in this local format since it enables the development of the flow within the duct to be more easily understood. The 5-hole probe area traverses provided local total and static pressures in addition to the velocity vector. Therefore, at a given plane, spatially averaged values can be obtained through suitable averaging techniques. The spatially averaged velocity normal to the traverse plane ($\bar{U}$) was obtained by area weighting the individual values while the total ($\tilde{P}$) was mass weighted such that:

$$\tilde{P}=\tilde{p}+\alpha\tfrac{1}{2}\rho\bar{U}^2 \quad \text{and} \quad \alpha=\frac{1}{A}\int^{A}\left(\frac{u}{\bar{U}}\right)^3 \qquad (2)$$

Where α is the kinetic energy coefficient and compares the kinetic energy flux of the actual profile to a uniform profile with the same mass flow. Hence, changes in the spatially averaged pressures between any two planes can then be expressed in terms of a total pressure loss (λ) and static pressure rise coefficient (Cp), with the change in pressures being non-dimensionalised by a suitable reference dynamic pressure.

$$\lambda=\frac{\tilde{P}_1-\tilde{P}_2}{\tilde{P}_1-\tilde{p}_1} \quad \text{and} \quad Cp=\frac{\tilde{p}_2-\tilde{p}_1}{\tilde{P}_1-\tilde{p}_1} \qquad (3)$$

In this way, for example, the mass-weighted duct loss can be obtained using the duct inlet (plane '1') and duct exit (plane '2') traverse plane data.

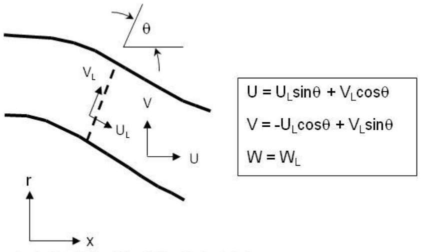

Figure 13: Local Co-ordinate System

The general accuracy of the rig hub and casing dimensions was measured, typically, to be of order 0.1mm and at each traverse plane the traverse height was also measured and found to be within 0.2% of that specified. The positional accuracy of the 5-hole pressure probe was within 0.1mm radially and 0.1° circumferentially and the pressures measured were estimated to be accurate to within 1%. The total velocity of the flow was obtained from the dynamic pressure, and hence the accuracy of the local velocities was within ±0.5%. While the pitch angle of the flow was determined from the calibration of the probe, additional errors in yaw angle could arise associated with the ability of the user to align the probe with the rig centre line. It is estimated that this could be set to within 1°, and this level of accuracy was reflected in the measured swirl angles and circumferential component of velocity. In addition to the errors associated with the local measurements it was estimated that the mass weighted total and static pressures at a given traverse plane were repeatable to better than 10Pa. The calculated mass flows at each traverse plane, derived from the velocity measurements, were all within 2.5% of each other.

RESULTS AND DISCUSSION

An aim of the integrated OGV concept was to maintain the rotor exit pressure field such that the rotor performance was unaffected. In a circumferentially averaged sense this is broadly the case as shown by the profiles presented in Figure 14.

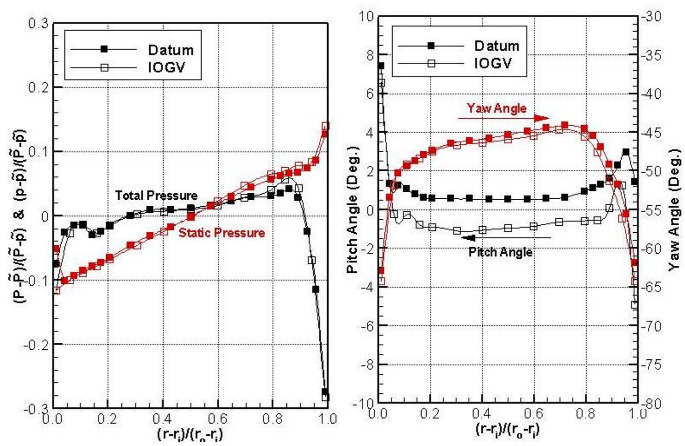

Figure 14: Circumferentially Averaged Profiles at Rotor Exit

However, examination of the contours presented in Figure 15 reveals some small differences in the structure of the mean flow field. At rotor exit/OGV inlet the flow is influenced by (i) remnants of the wake from the upstream IGV row and (ii) the upstream pressure field from the downstream OGV row. For the datum, the total pressure contours show evidence of the IGV wake and the static pressure contours contain a strong variation generated by the local pressure field associated with each OGV blade. This, in turn, results in a variation in the velocity field which clearly indicates an imprint of the OGV. For the integrated design, the lean and sweep of the OGV means the local influence of the upstream static pressure field at rotor exit is much reduced. As in the datum case the total pressure field is dominated by the IGV wake (which is most evident in the bottom right of the plot and stretches towards the top left). However, the leading edge sweep of the IOGV increases the distance between the rotor and the OGV (refer to Figure 11). This reduces the static pressure field associated with the downstream OGV and means that the variations in the velocity field are also dominated by the IGV wake effects.

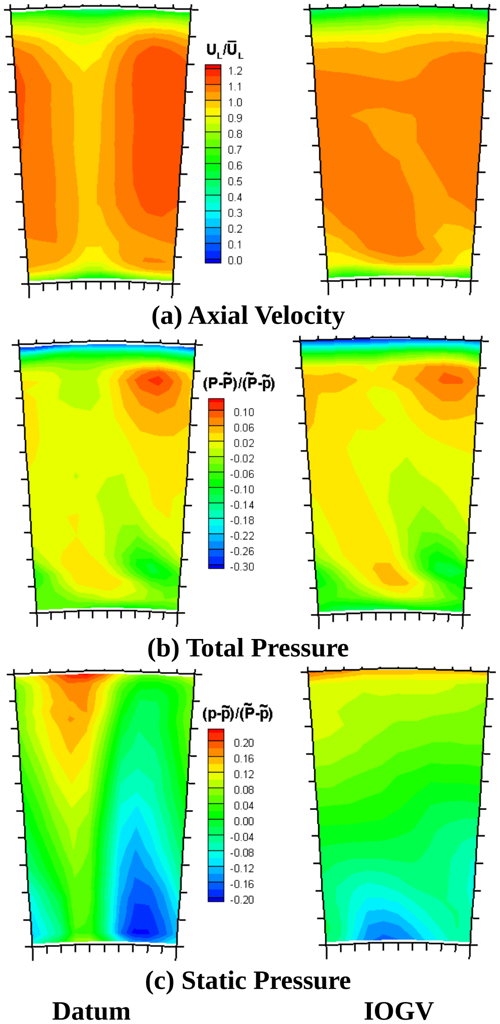

Figure 15: Contours at Rotor Exit

At OGV exit/duct inlet it is not surprising that the mean flow is dominated by the wake from the OGV as shown in Figure 16. In both cases the wakes suggest a well behaved blade row with no significant regions of separated flow. In addition, previous work[9] indicated that rather than high loss fluid being concentrated in specific loss cores, close to the hub and tip regions, the use of blade lean results in this fluid being distributed along the length of the blade. Comparing the total pressure contours shows some evidence of this occurring here. For the datum, the contours of static pressure also show the effect of the downstream geometry and the reduction in static pressure towards the hub reflecting the curvature of the flow as it anticipates the first bend. However, for the integrated design the OGV exit plane is actually downstream of the first bend and the static pressure is relatively flat. Given the different location of the OGV exit plane it is difficult to make further comparison of the mean flow fields at OGV exit. The measured OGV exit data and the design CFD (Figure 7) show a good level of agreement. The boundary layer and wake development are similar. Some subtle differences are apparent in the flow field but may just be a result of using a mixing plane at rotor exit in the CFD model. This transfers only a circumferentially averaged profile removing the IGV wake and its influence locally on the OGV.

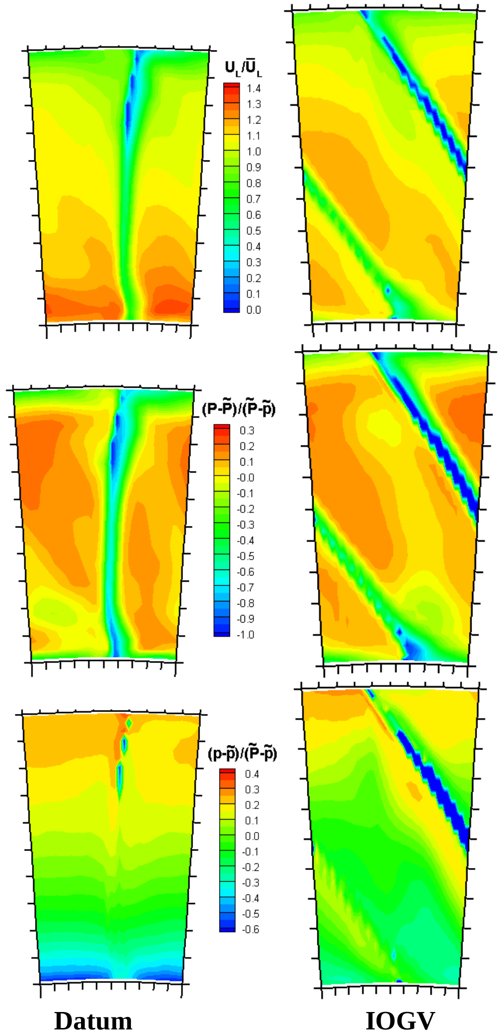

Figure 16: Measured Contours at OGV Exit

Downstream of the OGV the subsequent development of the flow field is highlighted by data obtained at various traverse planes. The wakes from the OGV can be observed throughout the transition duct as they mix out. Inevitably this leads to differences between the two designs as the wakes from the IOGV design are inclined compared to the datum. Further, the distance available for the wakes to mix out is reduced for the shorter integrated design, and the pressure field in which this mixing occurs is different. For the datum duct the initial mixing of the wake occurs in the first bend where a radially inward pressure gradient leads to a radial redistribution of the low momentum wake fluid towards the inner casing. However, despite these differences the bulk characteristics of the flow field appear broadly comparable. Comparison of circumferentially averaged profiles (Figure 17) throughout the ducts shows a good level of similarity. Downstream of plane D the mid-passage (core) flow exhibits the same level of profile distortion which is purely a function of the duct curvature. In the viscous affected outer wall region the boundary layer growth is comparable with a boundary layer thickness at duct exit of order 5-10% of passage height. More importantly, on the critical inner wall the data suggest that there is perhaps a reduced tendency for separation despite the shorter system length of the integrated configuration. At planes F-H the inflection of the profile for the datum suggests a shape factor in excess of 2.2 and the very close proximity of separation. For the integrated design the inflection is removed although the profiles still suggest a relatively high shape factor.

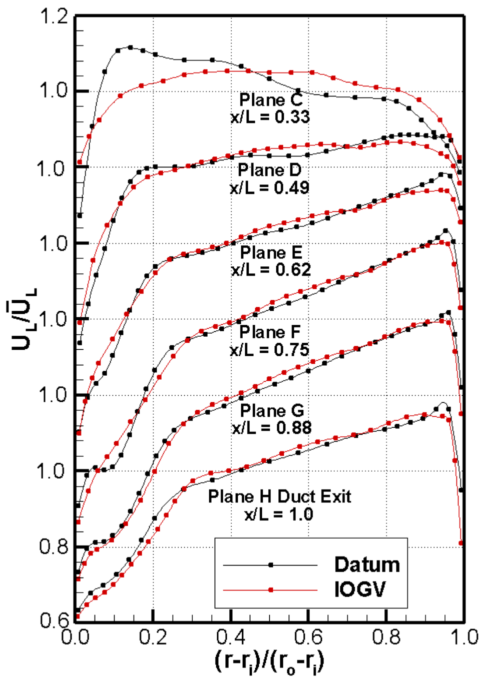

Figure 17: Circumferentially Averaged Profiles of Normal Velocity

This is also seen in the wall static pressure distributions (Figure 18) which reflect the curvature being undertaken by the flow and the axial pressure gradients to which the casing boundary layers are being subjected. It might be assumed that flow separation is most likely to occur at the point of maximum pressure close to plane F but inspection of the velocity contours suggest that the flow is closest to separation slightly upstream of this at plane E (Figure 19). This is due to the impact of streamline curvature which, along the inner casing, will suppress and then enhance the production of turbulence within the first and second bends of the ducts respectively. Turbulence suppression in the first bend reduces the exchange of momentum close to the casing surface making the flow more prone to separate. However, the turbulent enhancement in the second bend increases this beneficial momentum exchange, although it takes some distance (~ order of 2 boundary layer heights) for this to be observed in the mean velocity field. This combination of pressure gradient and flow curvature effects results in the flow being closest to separation at plane E. However the normal velocity contours at this plane, shown in Figure 19, are in line with the aggressive nature of the ducts, i.e. the high aerodynamic loading has resulted in the flow field being close to, but not actually, separated. At duct exit the measured velocity contours presented in Figure 20 suggest that the level of mixing, the depth of the wakes and the overall level of non-uniformity are comparable between the datum and integrated designs.

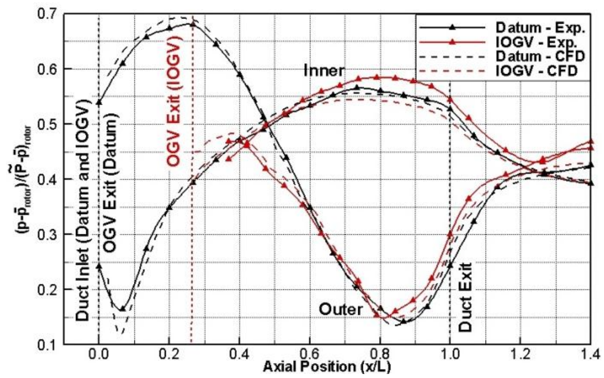

Figure 18: Wall Static Pressure (S-duct inlet at x/L = 0)

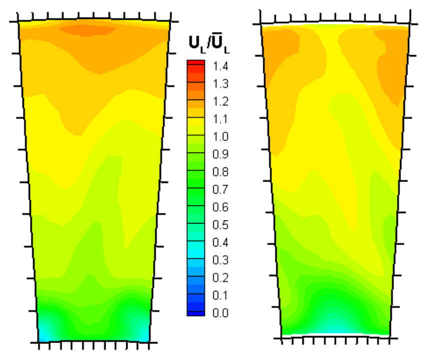

(a) Datum (b) IOGV

Figure 19: Measured Normal Velocity Contours at Plane E

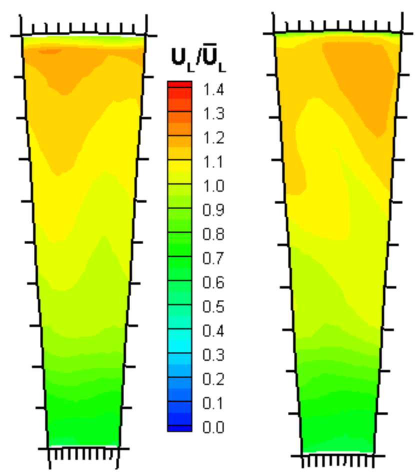

(a) Datum (b) IOGV

Figure 20: Measured Velocity Contours at Duct Exit

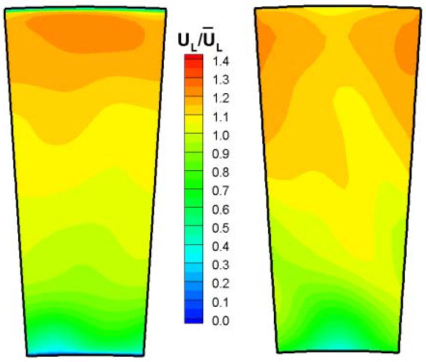

(a) Datum **(b) IOGV**

Figure 21: Post-Test Predicted Velocity Contours at Plane E

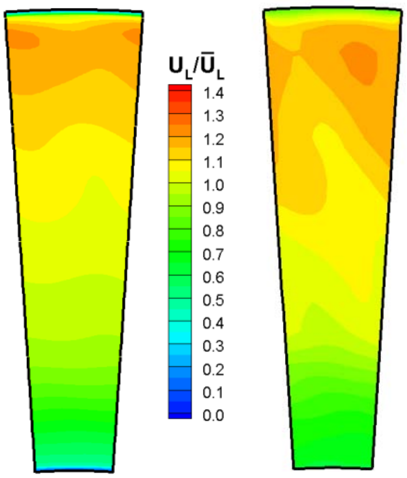

(a) Datum **(b) IOGV**

Figure 22: Post-Test Predicted Velocity Contours at Exit

The pre-test CFD (Figures 9 and 10) shows an adequate agreement with the measured data (Figures 19 and 20) and, in terms of a design tool, achieves its goal in assessing the basic flow field and aerodynamic loading prior to committing to test. Nonetheless, the pre-test predictions exhibit a slight shift in the radial position of the peak velocity and a slight increase in the degree of mixing. This is due mainly to the specification of the inlet boundary condition which used data from the compressor design CFD to directly specify the three components of velocity and estimate the turbulence. However, the measured flow field at the OGV exit differs slightly to that predicted by the compressor design CFD. It is difficult to say whether this results from numerical errors in the prediction (i.e. turbulence model or the use of a mixing plane between the rotor and OGV) or some degree of experimental error. The use of measured velocity and turbulence data to specify the inlet condition for a post-test prediction produces a much better agreement between the experiment and CFD. The general structure of the flow field, the level of mixing and the depth of the wakes are now well represented at both plane E and duct exit (see Figures 21 and 22). It should be noted that in deriving the turbulence intensity and length scale from the measurements the rotor passing frequency was removed using the method of Camp and Shin[17]. In this way the mean turbulence was a true reflection of the mean flow field and not artificially increased by the rotor passing frequency and its harmonics.

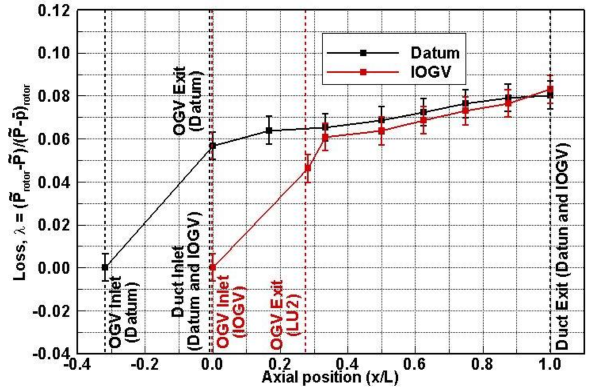

Figure 23: Development of Loss Along the Ducts (S-duct inlet at x/L = 0)

In terms of overall performance the system mass-weighted total pressure loss coefficients are presented in Table 2 (with reference to rotor exit) and the development of this loss through the S-shaped ducts is plotted in Figure 23. Surprisingly the loss over the OGV is slightly reduced for the integrated design (4.6% of rotor exit dynamic pressure as opposed to 5.8%). It could be assumed that the lean and sweep would increase aerodynamic loading and loss but it would appear that the detailed design process of integrating the OGV within the static pressure field has actually improved the performance and reduced the loss. The overall system total pressure loss for the datum and IOGV designs is comparable at approximately 8% of the rotor exit dynamic pressure.

	$\lambda_{rotor\text{-}ogv\ exit}$	$\lambda_{rotor\text{-}duct\ exit}$
Datum	0.058	0.080
IOGV	0.046	0.083

Table 2: Measured Loss Coefficients

CONCLUSIONS

A numerical design methodology has been successfully employed in order to integrate an OGV row into the first bend of an aggressive S-shaped compressor transition duct. Although the duct itself was similar in geometry, integration results in a 21% reduction in system length compared to a conventional datum design. Both ducts were experimentally evaluated on a fully annular low-speed test rig demonstrating that (i) the integration process was transparent to the rotor performance; (ii) the integrated design exhibited a similar level of aerodynamic loading along the critical inner wall despite the reduction in system length; and (iii) the duct exit profiles were identical. The total pressure loss across the OGV was slightly reduced due to better matching vane row to the flow field. The overall system loss was comparable indicating a slight increase in loss in the duct (probably due to the increased mixing associated with the longer skewed wakes of the integrated design).

ACKNOWLEDGMENTS

The authors wish to acknowledge the financial support of the European Commission. This work was conducted within the EU 6th Framework Project AIDA (Aggressive Intermediate Duct Aerodynamics for Competitive and Environmentally Friendly Jet Engines – Contract No. AST3-CT-2003-502836).

REFERENCES

[1] Bradshaw, P., "The Effects of Streamline Curvature on Turbulent Flow", AGARD AG-169, 1973.

[2] Bailey, D. W., Britchford, K. M., Carrotte, J. F. and Stevens, S. J., 1997, "Performance Assessment of an Annular S-Shaped Duct", ASME Journal of Turbomachinery, Vol. 119, pp 149-156.

[3] Karakasis, M. K., Naylor, E. M. J., Miller, R. J., and Hodson, H. P., 2010, "The Effect of an Upstream Compressor on a Non-Axisymmetrc S-Duct", ASME GT2010-23404.

[4] Carrotte, J. F., Stevens, S. J. and Wray, A. P., 1990, "The Performance of a Combustor Pre-diffuser Incorporating Compressor Outlet Guide Vanes", AIAA-90-2165.

[5] Walker, A. D., Carrotte, J. F. and McGuirk, J. J., 2007, "Enhanced External Aerodynamic Performance of a Generic Combustor Using and Integrated OGV/Pre-Diffuser Design Technique", ASME Journal of Engineering for Gas Turbines and Power, Vol. 129(1), pp 80-87.

[6] Britchford, K. M., Manners, A. P., McGuirk, J. J. and Stevens, S. J., 1994, "Measurement and Prediction of Flow in Annular S-Shaped Ducts", Journal of Experimental Thermal and Fluid Science, 9(2), pp 197-205.

[7] Smith, L. H., 1974, "Some Aerodynamic Design Considerations for High Bypass Ratio Fans", 2nd Int. Symposium on Air Breathing Engines, Sheffield, UK.

[8] Wadia, A. R., Szucs, P. N., and Gundy-Burket, K. L., 1998, "Design and Testing of Swept Leaned Outlet Guide Vanes to Reduce Stator-Strut-Splitter Aerodynamic Flow Interactions", ASME 98-GT-70.

[9] Britchford, K. M., Carrotte, J. F., Kim, J. H. and Hield, P. M., 2001, "The Effect of Operating Conditions on the Aerodynamic Performance of an Integrated OGV S-Shaped Duct", ASME 2001-GT-0347.

[10] Denton, J. D., and Xu, L., 1998, "The Exploitation of 3D Flow in Turbomachinery Design", IMechE Journal of Mechanical Engineering Science, Part C.

[11] Gallimore, S. J, Bolger, J. J., Cumpsty, N. A, Taylor, M. J., Wright, P. I., and Place, J. M. M., 2002, "The Use of Sweeo and Dihedral in Multistage Axial Flow Blading – Part 1: University Research and Methods Development", ASME Journal of Turbomachinery, Vol. 124(4), pp 521-523.

[12] Youngren, H., and Drela, M., 1991, ''Viscous/Inviscid Method for Preliminary Design of Transsonic Cascades,'' Paper No. AIAA-91-2364.

[13] Lapworth L., Shahpar S., 2004, "Design of Gas Turbine Engines using CFD", ECCOMAS 2004, Eds., Neittannmaki, et al., Finland.

[14] Ortiz-Duenas, C., Miller, R. J., Hodson, H. P., and Longley, J. P., 2007, "Effect of Length on Compressor Inter-Stage Duct Performance", ASME GT2007-27752.

[15] Cumpsty, N. A., 1989, "Compressor Aerodynamics." Longman Scientific and Technical.

[16] Wray, A. P. and Carrotte, J. F., 1993, "The Development of a Large Annular Facility for Testing Gas Turbine Combustor Diffuser Systems", AIAA-93-2546.

[17] Camp, T. R. and Shin, H. –W., 1995, "Turbulence Intensity and Length Scale Measurements in Multistage Compressors", ASME Journal of Turbomachinery, Vol. 117(1), pp. 38-46.